J Mater Sci (2008) 43:3717–3724
DOI 10.1007/s10853-008-2604-3

Dynamic and metadynamic recrystallization of Hastelloy X superalloy

M. Aghaie-Khafri · N. Golarzi

Received: 13 February 2008 / Accepted: 20 March 2008 / Published online: 4 April 2008

Abstract Hot compression tests in the temperature range of 900–1150 °C and strain rates varying between 0.001 and 0.5 s^{-1} were performed on Hastelloy X superalloy in order to investigate the kinetics of hot deformation. An Arrhenius-type equation was used to characterize the dependence of the flow stress on deformation temperature and strain rate. The results showed that dynamic recrystallization (DRX) as well as metadynamic recrystallization (MDRX) occurred during hot working. A novel technique has been developed for calculating the DRX kinetics parameters on the basis of the Johnson-Mehl-Avrami-Kolmogorov (JMAK) and isothermal transformation rate equations. The variation of grain size in the DRX and MDRX regimes correlated with the standard Zener–Hollomon parameter.

Introduction

Nickel-base superalloys are among the most difficult engineering materials to fabricate via deformation-processing techniques. The high temperature mechanical properties of these alloys are highly sensitive to the flow characteristic and the microstructural changes of the material during hot working. In hot forming of metals at temperatures above the recrystallization temperature, the influence of strain rate becomes increasingly important. The strain rates for industrial processing [1] are higher than those for either DRX or superplasticity and give rise to transient regimes like dynamic recovery and MDRX depending on the temperature [2].

M. Aghaie-Khafri (✉) · N. Golarzi
Faculty of Mechanical Engineering, K.N. Toosi University of Technology, P.O. Box 19395-1999, Tehran, Iran
e-mail: maghaei@kntu.ac.ir

Hastelloy X is a wrought superalloy widely used in gas turbines as combustors, transition pieces, exhaust-end components, and so on [3]. Although a number of studies have focused on the hot deformation behavior of Ni-base superalloys and various empirical equations for prediction of grain size have been proposed [4–7], a few reports dealt with the flow behavior of Hastelloy X [8–11]. Castelli et al. [8] showed that this alloy exhibits a strong isothermal strain aging peak at approximately 600 °C promoted by the combined effects of solute drag and precipitation hardening. Their results clearly revealed that the deformation behavior of Hastelloy X is thermomechanically path dependent. The viscoplastic behavior of Hastelloy X was characterized using the Bodner-Parton unified constitutive model [9] and a viscoplastic constitutive model was presented for the estimation of the overall mechanical response of the polycrystalline alloy [10]. Isothermal cyclic deformation and the mechanisms contributing to the observed marked cyclic hardening in Hastelloy X were investigated by Rowley and Thornton [11].

Despite the studies conducted in the past, in the present investigation kinetics of high temperature deformation of Hastelloy X was studied by means of hot compression experiments and microstructural evaluation. In addition, the variation of microstructure due to DRX, MDRX, as well as grain growth was considered.

Experimental procedures

Materials and lubricants

The chemical composition of the starting material used in this investigation is listed in Table 1. The raw material was produced by vacuum melting process and it was hot forged

Table 1 Chemical composition of the material used in this study in wt%

C	Mn	Si	Cr	Mo	Ti	Al	W	Co	Fe	Ni
0.17	0.7	0.35	22.72	8.12	0.176	0.05	0.43	0.99	17.35	Bal.

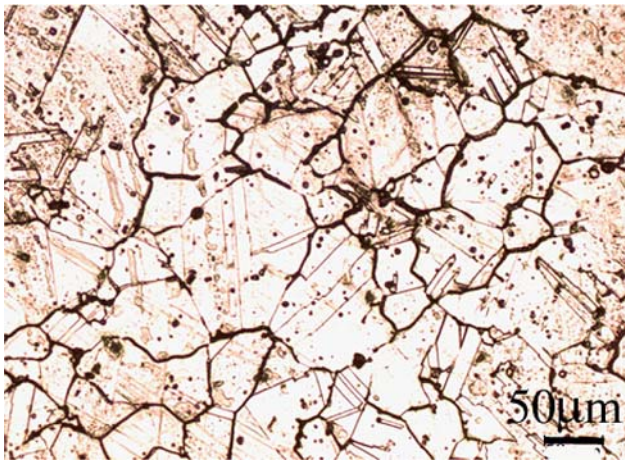

Fig. 1 Microstructure of the as-received material

to remove the casting structure. The microstructure of the as-received material is shown in Fig. 1 and the average grain diameter was 95 μm. Cylindrical specimens with a 5-mm diameter and 7.5-mm height were machined out of the as-received stock.

The choice of lubricant depends on the processing conditions, the characteristics of the tooling and work piece, and the operating or interfacial temperature, with the latter probably having the greatest influence on the lubricant selection [12]. A number of lubricants having high temperature stability, namely boron nitride, Deltaglaze, graphite, glass powder, and mica were examined in this work. The results showed that a combination of glass powder, graphite, and mica sheet gave the lowest flow stress values and minimized the barreling of the specimens. Consequently, a combination of glass powder and mica sheet at both ends of the specimens together with a layer of graphite powder at the interface of anvil and mica sheet was used as lubricant.

Hot compression testing

Compression testing was accomplished in an Instron 8503 computer controlled servo hydraulic testing machine. A resistance heating split furnace, which was interfaced with a digital programmer and controller, was used to surround the CMS1810 superalloy anvils and specimen. A small hole was drilled at midheight of the specimen for inserting a thermocouple which is used to measure the actual temperature of the specimen as well as adiabatic temperature rise if any during testing [13].

Hot compression experiments were conducted at constant true strain rates of 0.001, 0.01, 0.1, and 0.5 s^{-1} and at temperatures of 900, 950, 1000, 1050, 1100, and 1150 °C. Each of the samples was heated to temperature in ~5 min, was held at the deformation temperature for 5 min to eliminate the thermal gradient, and was then deformed to total true strain of 0.7. Samples were quenched in water after hot deformation to capture the microstructure of the hot deformed material. The time between the end of deformation and the moment when specimens were quenched in water was 1–3 s.

In each test, the load-stoke data were converted into true stress–true plastic strain data after making corrections for friction using the following equation [14]:

$$\frac{P}{\sigma} = \left(\frac{h}{4\mu a}\right)^2 \left(e^{2\mu a/h} - \frac{2\mu a}{h} - 1\right), \quad (1)$$

where σ is the friction corrected flow stress, P the uncorrected flow stress, a and h are instantaneous radius and height of specimen, and μ is the friction coefficient which was determined according to the amount of barreling for each specimen [12].

The stress–strain curves at strain rates of 0.1 and 0.5 s^{-1} and at temperatures of 900–1050 °C were corrected for deformation heating. Adiabatic temperature rise was recorded using a transient oscilloscope. Finally, at a given value of ε and T, the softening, $\Delta\sigma$, due to measured ΔT was calculated, assuming a linear variation of log σ with $1/T$, and added to the as-measured value of σ to obtain the isothermal value [15].

Microstructure evaluation

It is worth noting that for the determination of grain size, the specimens were sectioned at midplane parallel to the compression axis and the cut surface was prepared for metallographic investigation using conventional techniques. Subsequently, the specimens were etched with Kalling solution. Grain size of specimens was measured using the intercept method given in ASTM E112.

An image analysis software, Clemex, was used for image processing. The software uses the binarization processing, that is each pixel has an intensity value ranging from 0 to 250 and a specific range of pixels are assigned binary values that the computer can manipulate. The area fraction of recrystallized grains was calculated by the combination of automated classification of different grains based on their size and subsequent manual designation of recrystallized one.

Results and discussion

Stress-strain curve and microstructure

Typical stress–strain curves obtained at 900, 1050, 1100 °C and at the different strain rates are shown in Figs. 2–5, respectively. Stress-strain curves at 900 °C and strain rates of 0.001–0.1 s^{-1} show flow stress softening. For all the conditions, the flow stress reached steady state at strains greater than about 0.3. The stress-strain curve at strain rate of 0.5 s^{-1} shows a peak stress followed by a continuous decrease in the flow stress. Deformation at 900 °C, except at a strain rate of 0.5 s^{-1}, resulted in a microstructure with elongated grains, which are typical of dynamic recovery. One such microstructure is shown in Fig. 6, which corresponds to the specimens deformed at 900 °C and strain rates of 0.01 and 0.1 s^{-1}.

The flow curves for deformation at 1050 (Fig. 3) and 1100 °C (Fig. 4) show flow softening at each strain rate investigated, and beyond the critical strain for the peak

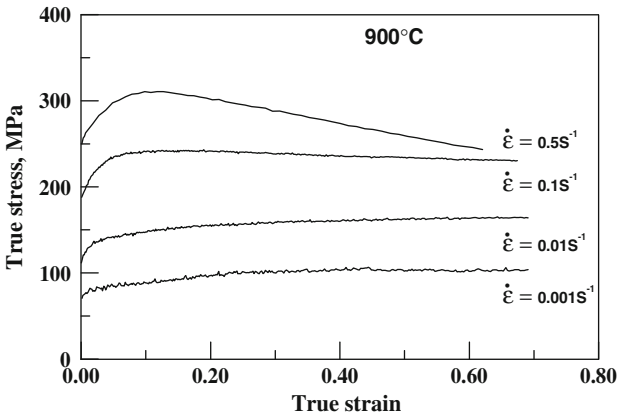

Fig. 2 True stress–true strain curves at 900 °C and different strain rates

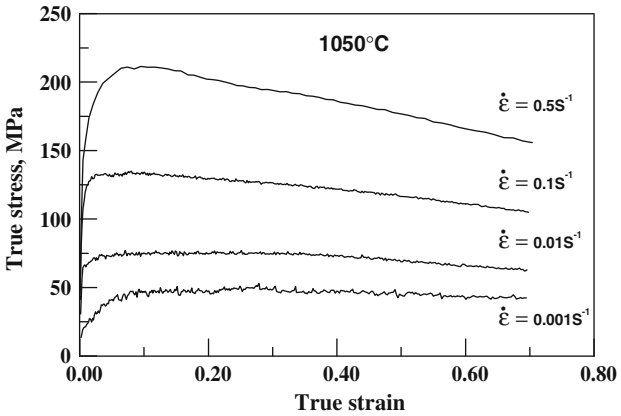

Fig. 3 True stress–true strain curves at 1050 °C and different strain rates

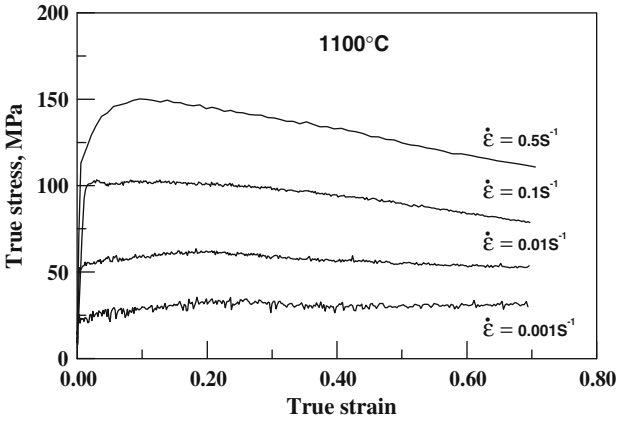

Fig. 4 True stress–true strain curves at 1100 °C and different strain rates

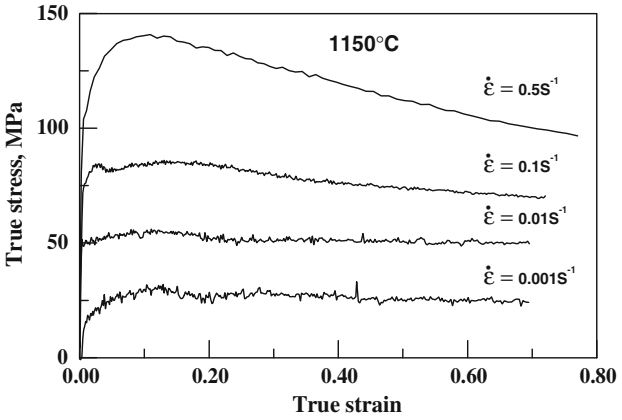

Fig. 5 True stress–true strain curves at 1150 °C and different strain rates

stress, the flow stress decreased with increasing strain. Multiple stress peaks were observed in the flow curves for deformation at low strain rates which is especially evident at 1100 °C. At higher strain rates, a single peak stress was observed especially for 0.5 s^{-1}.

The microstructure of Hastelloy X deformed at 1050 °C and 0.5 s^{-1} is shown in Fig. 7, which exhibits typical DRX features and the near absence of annealing twins. The microstructures of the specimens deformed at 1100 and 1150 °C with different strain rates of 0.01–0.5 s^{-1} have features typical of MDRX. One such microstructure is shown in Fig. 8, which corresponds to a specimen deformed at 1150 °C and a strain rate of 0.1 s^{-1}. The microstructure consisted of equiaxed grains with straight grain boundaries as well as with annealing twins, which are similar to those obtained by post deformation recrystallization. As the rate of MDRX is much faster than of normal static recrystallization, there is no incipient time period for the nucleation of recrystallized grains. Furthermore, although DRX is simply described as a function of strain

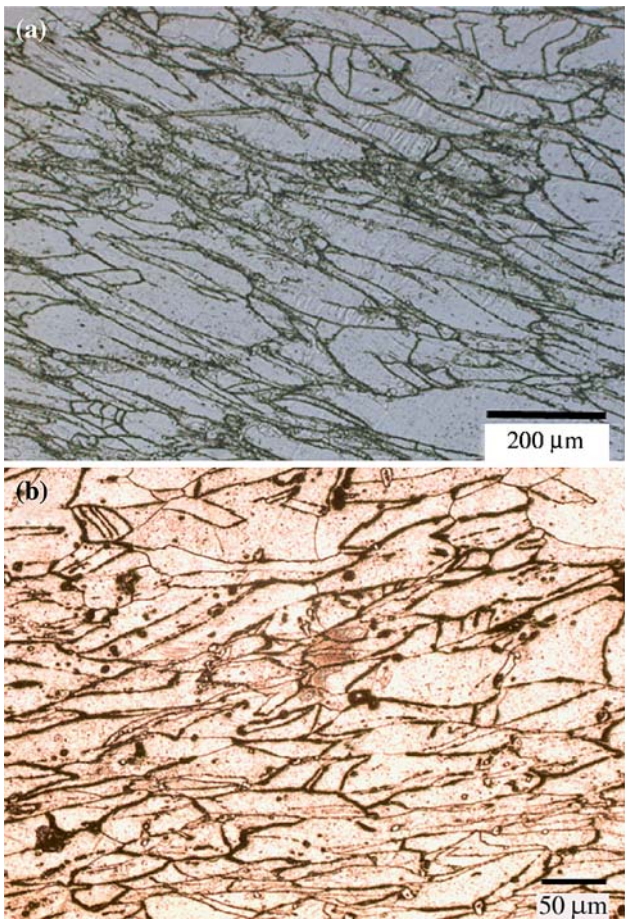

Fig. 6 Microstructure of Hastelloy X specimens deformed at 900 °C and strain rate of (**a**) 0.01 $s^{-1}$and (**b**) 0.1 s^{-1}

Fig. 7 Microstructure of the sample deformed at temperature of 1050 °C and strain rate of 0.5 s^{-1}

rate and temperature, MDRX is rather a function of grain size and strain. It may be conjectured that MDRX is closely related to the density of unrecoverd dislocations accumulated within the grains [16].

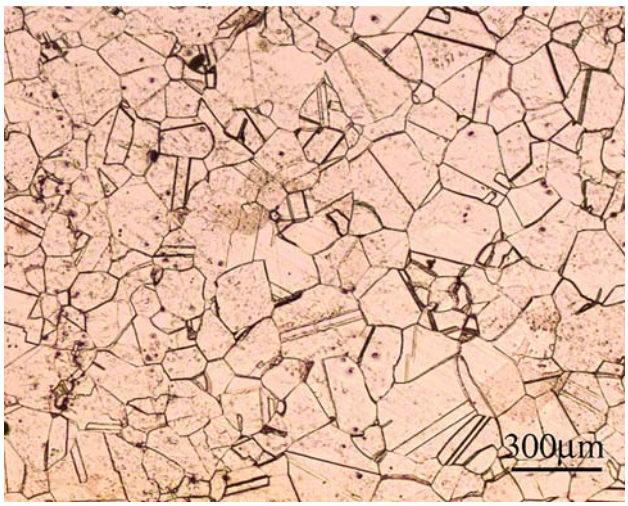

Fig. 8 Microstructure of the sample deformed at temperature of 1150 °C and strain rate of 0.1 s^{-1}

In the present investigation, in which the Hastelloy X specimens were deformed to a strain of 0.7 and the holding time after the end of deformation was about 1 s, MDRX was observed to have the following feathers. MDRX was observed at temperatures above 1050 °C and strain rates greater than 0.001 s^{-1}, as indicated in Fig. 9. However, only a few percent ($\sim$5%) of MDRX grains were observed at a strain rate of 0.001 s^{-1} and different temperatures of 1050–1150 °C. Also, comparison of the grain size in the specimens deformed at the same strain rate but with different deformation temperatures (1100 and 1150 °C) indicates that the MDRX grain size increases with increasing temperature, as shown in Fig. 9.

Constitutive relation

During high temperature deformation, the relationship between the steady state flow stress, strain rate, and temperature is generally expressed in the form of a rate equation given by:

$$\sigma = B\dot{\varepsilon}^m \exp\left(\frac{mQ}{RT}\right) = BZ^m, \tag{2}$$

where the quantity $Z = \dot{\varepsilon}\exp\left(\frac{Q}{RT}\right)$ is frequently referred to as the temperature-compensated strain rate or the Zener–Hollomon parameter, B is a constant, m is the strain rate sensitivity, and Q is the apparent activation energy for hot deformation. If Eq. 2 adequately represents the constitutive behavior of Hastelloy X, then a log–log plot of the flow stress versus the Zener–Hollomon parameter should yield a straight line with a slope of m. The value of m is defined by:

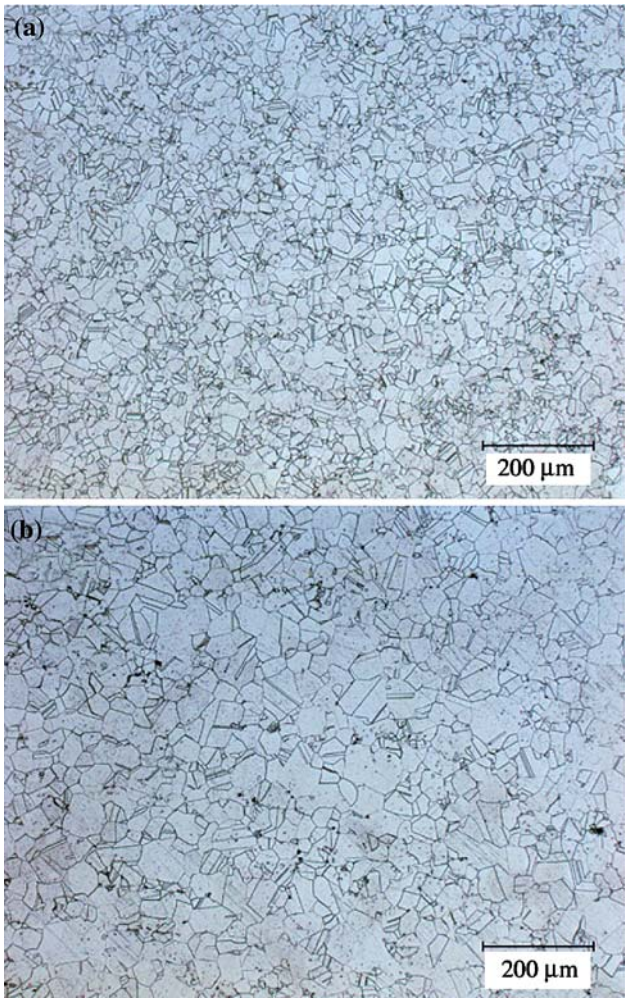

Fig. 9 Microstructure of the samples deformed at (**a**) temperature of 1100 °C and strain rate of 0.5 s^{-1}, (**b**) temperature of 1150 °C and strain rate of 0.5 s^{-1}

$$m = \left.\frac{\partial \ln \sigma}{\partial \ln \dot{\varepsilon}}\right|_{T,\varepsilon}, \tag{3}$$

and can be calculated from a plot of $\ln(\sigma)$ versus $\ln(\dot{\varepsilon})$, as shown in Fig. 10. It is clear that the value of m changes from 0.11 at 950 °C to 0.22 at 1150 °C. Furthermore, m increases with temperature and an abrupt increase occurs at 1000 °C. The phenomenon can be attributed to DRX at higher temperatures that produces a higher strain rate sensitivity [17]. From Eq. 2, the activation energy Q, may be defined by:

$$Q = \frac{R}{m}\left.\frac{\partial \ln \sigma}{\partial (1/T)}\right|_{\dot{\varepsilon},\varepsilon}, \tag{4}$$

and is computed from the slopes of the plots shown in Fig. 11. The mean apparent activation energy for Hastelloy X was calculated to be 370 kJ/mol, which is comparable to previously reported values for other superalloys [18].

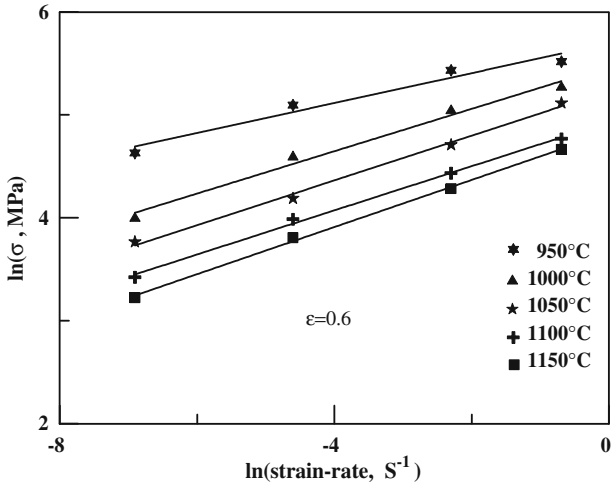

Fig. 10 Plot of $\ln(\sigma)$ versus $\ln(\dot{\varepsilon})$ at a strain of 0.6

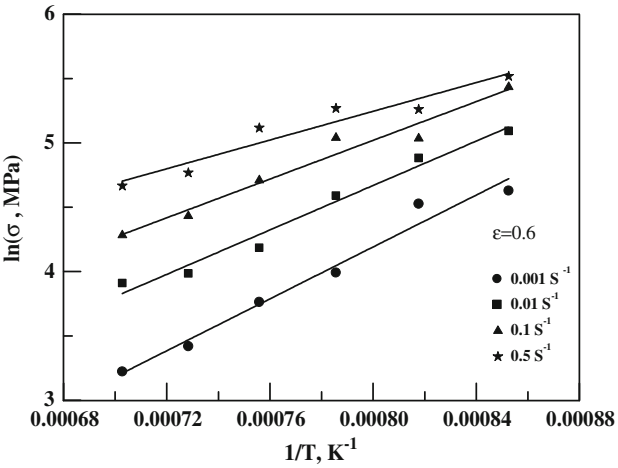

Fig. 11 Plot of $\ln(\sigma)$ versus $1/T$ at a strain of 0.6

The apparent activation energy value determined above was used to calculate the Zener-Hollomon parameter, which is plotted versus the flow stress in Fig. 12. This plot shows a good correlation between the flow stress and the Zener–Hollomon parameter which implies that the flow stress follows the expected trend with respect to strain rate and temperature.

Kinetics of recrystallization

Concerning the kinetics of DRX, the fraction of dynamically recrystallized grains at a strain rate of 0.001 s^{-1} for different temperatures was determined, as shown in Fig. 13. The fraction of recrystallized grains was found to increase with deformation temperature at a given strain rate.

The kinetics of phase transformation involving nucleation and growth under isothermal conditions can be described by the JMAK equation:

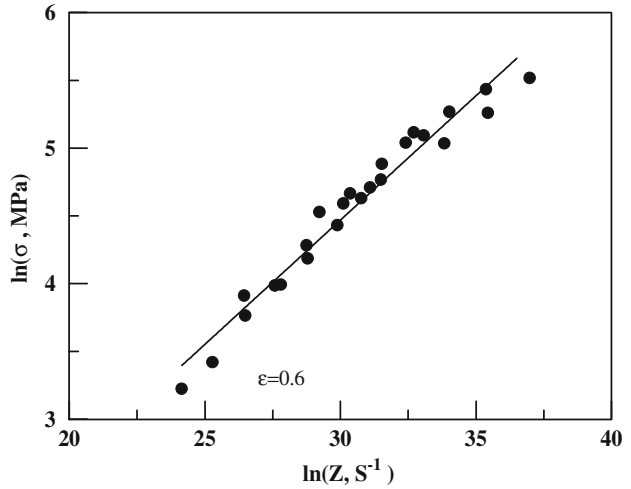

Fig. 12 Variation of flow stress versus Zener–Holomon parameter at a strain of 0.6

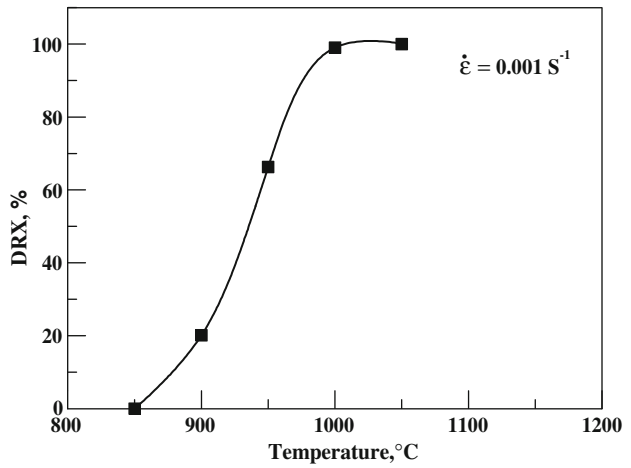

Fig. 13 Fraction of recrystallized grains as a function of deformation temperature

$$X(t) = 1 - \exp\left(-Kt^n\right), \tag{5}$$

where X is the fraction of the transformation completed at time t; K is a function of the temperature and in general depends on both the nucleation rate and the growth rate; and n is a parameter which reflects the nucleation rate or the growth morphology. The temperature dependence of K is usually described as:

$$K = K_0 \exp\left(-\frac{E}{RT}\right), \tag{6}$$

where E is the appropriate activation energy and R is the gas constant. Taking the logarithm of both sides in Eq. 5 and inserting into Eq. 6 gives:

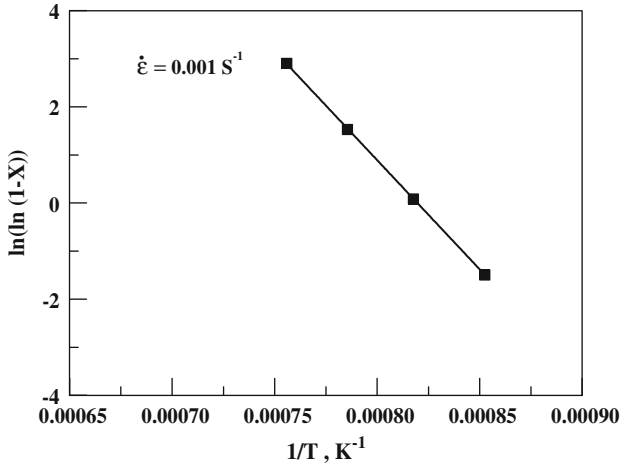

Fig. 14 A plot of $\ln(\ln(1/(1-X)))$ versus $1/T$

$$\ln\left(\ln\left(1/1-X\right)\right) = \ln K_0 - \frac{E}{RT} + \ln t^n. \tag{7}$$

A plot of $\ln(\ln(1/(1-X)))$ versus $1/T$ should be approximately linear with a slope equal to $-E/R$, as shown in Fig. 14. The activation energy was calculated to be 375 kJ/mol for a strain rate of 0.001 s^{-1}, which is in close agreement the activation energy calculated using Eq. 4.

The isothermal transformation rate can be easily determined from Eq. 5 by differentiating with respect to time.

$$\frac{dX}{dt} = Knt^{n-1}\exp\left(-Kt^n\right). \tag{8}$$

Because of the explicit relation between X and t given by Eq. 5, Eq. 8 can be rewritten equivalently as:

$$\frac{dX}{dt} = nK^{1/n}(1-X)\left[\ln\left(1-X\right)^{-1}\right]^{(n-1)/n}. \tag{9}$$

Equation 9 is sometimes referred to as JMAK transformation rate equation. Concerning Eq. 6, it is possible to rewrite Eq. 9 [19]:

$$dX/dt = nK_0^{1/n}\exp\left(\frac{-E}{Rn}\frac{1}{T}\right)(1-X)\left[\ln\left(1-X\right)^{-1}\right]^{\frac{n-1}{n}}. \tag{10}$$

Taking the derivative of Eq. 10 with respect to $1/T$, gives [20]:

$$\frac{d\ln\left(dX/dt\right)}{d(1/T)} = -\frac{E}{nR} + \frac{d\ln\left\{(1-X)\left[\ln\left(1-X\right)^{-1}\right]^{\frac{n-1}{n}}\right\}}{d(1/T)}. \tag{11}$$

Henderson [19] assumes that the second term on the right hand side in Eq. 11 is small compared to the first one and a plot of $\ln(dX/dt)$ versus $1/T$ will approximate a

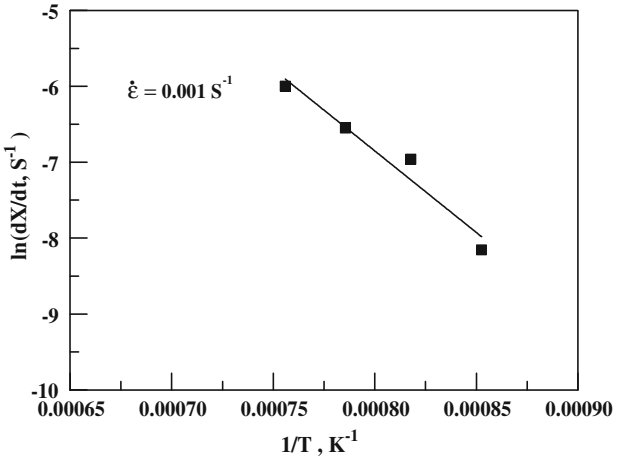

Fig. 15 Variation of ln(d*X*/d*t*) versus 1/*T*

straight-line behavior with a slope equal to $-E/nR$. Figure 15 shows the variation of ln(d*X*/d*t*) versus 1/*T* at different strain rates. The *n* value determined using an activation energy of 375 kJ/mol is about 1.8. For isothermal kinetics, when nucleation occurs heterogeneously at grain boundary edges and early site saturation assumes, the product phase grows essentially with cylindrical symmetry around the grain edges and an exponent of 2 is obtained [21]. However, studies on recrystallization have reported n values varying from 1 to 3 [22] and support the value of 1.8 determined for Hastelloy X.

Variation of grain size

It is generally accepted that there is a correlation between the grain size in the deformed samples and the temperature and the strain rate at a given strain [2, 16, 23]. The variations of the grain size versus *Z* and $\dot{\varepsilon}$ are shown in Figs. 16 and 17, respectively. It is clear that a straight-line relationship is valid for a specific deformation temperature. Under ideal situations, it is expected that all of the data points would lie on a single line within experimental scatter. The observed deviation is mainly due to post deformation recrystallization (MDRX) in the material. It is worth noting that the slope of the line ln(*d*) versus ln $(\dot{\varepsilon})$ in the MDRX regime is very small suggesting that the strain rate has a minor effect on the grain size. Under the conditions of MDRX, it is preferable to model the grain size evolution by using a dynamic state parameter like strain rate and a kinetic rate parameter representing the temperature dependence of grain size [2].

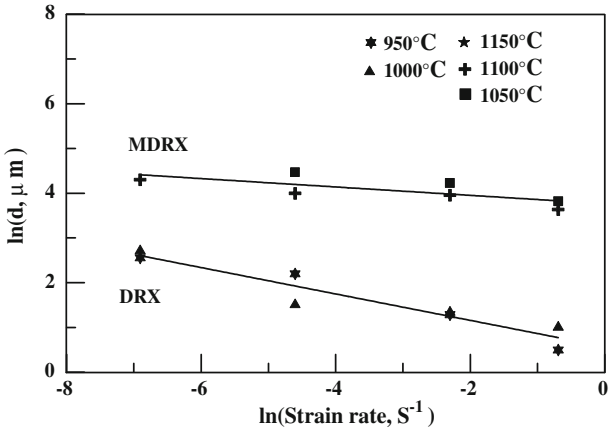

Fig. 17 A plot of the grain size versus $\dot{\varepsilon}$ for DRX and MDRX regimes

Figure 16 indicates that the transition from DRX to MDRX types of behavior happens over a very narrow temperature range of 1050–1100 °C. It is interesting to note that in wrought superalloys solution anneal is performed at temperatures above 1050 °C and dissolves γ' and carbide phases [24]. Consequently, the phenomenon

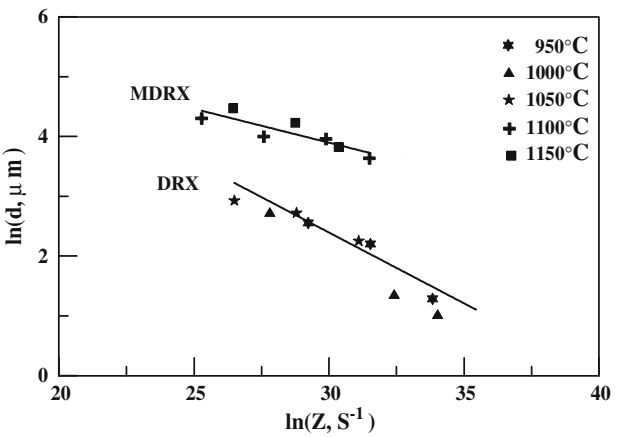

Fig. 16 Grain size diameter as a function of Zener–Holomon parameter

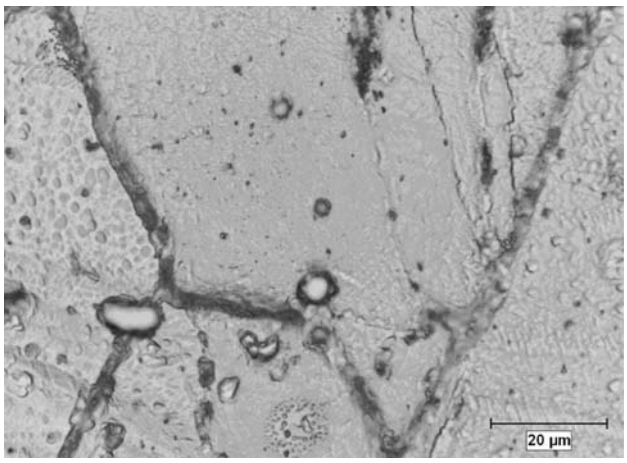

Fig. 18 Microstructure of the sample deformed at temperature of 1050 °C and strain rate of 0.01 s^{-1}

observed can be attributed to the second phases that are still stable at hot working temperatures around 1050 °C and prevent MDRX at low temperatures. This also causes the restriction of the grain boundary migration during DRX and formation of serrated and wavy-shape grain boundaries during hot deformation, as shown in Fig. 18.

Conclusions

The study of flow behavior of Hastelloy X superalloy over the strain rate range of 0.001–0.5 s^{-1} and the temperature range of 900–1150 °C leads to the following conclusions.

- The mean hot deformation apparent activation energy of 370 kJ/mol which was calculated from a plot of ln σ versus $1/T$ is comparable with the recrystallization activation energy calculated on the basis of JMAK equation and a plot of $\ln\ln(1/(1-x))$ versus $1/T$. Time exponent of 1.8 was obtained based on a plot of $\ln(dx/dt)$ versus $1/T$.
- MDRX occurs in the temperature range 1100–1150 °C and strain rate range 0.01–0.5 s^{-1} and results in microstructures similar to those of annealed material.
- The variation of grain size with the temperature and strain rate in the DRX and MDRX regimes can be correlated with Zener–Hollomon parameter. However, results obtained signify that strain rate has a minor effect on the MDRX grain size.

References

1. Wilkinson NA (1989) In: Loria EA (ed) 718 Metallurgy and applications. TMS, Warrendale, PA, p 119
2. Medeiros SC, Prasad YVRK, Frazier WG, Srinivasan R (2000) Mater Sci Eng A 293:198. doi:10.1016/S0921-5093(00)01053-4
3. Zhao JC, Larsen M, Ravikumar V (2000) Mater Sci Eng A 293:112. doi:10.1016/S0921-5093(00)01049-2
4. Srinivasan N, Prasad YVRK (1994) Metall Trans A 25:2275. doi:10.1007/BF02652327
5. Zhang JM, Gao ZY, Zhuang JY, Zhong ZY (1999) J Mater Proc Tech 88:244. doi:10.1016/S0924-0136(98)00401-4
6. Yuan H, Liu WC (2005) Mater Sci Eng A 408:281. doi:10.1016/j.msea.2005.08.126
7. Semiatin SL, Fagin PN, Glavicic MG, Raabe D (2004) Scri Mater 50:625. doi:10.1016/j.scriptamat.2003.11.030
8. Castelli MG, Miner RV, Robinson DN (1993) In: Proceedings of the Symposium on Thermomechanical Fatigue Behavior of Materials. ASTM, Philadelphia, p 106
9. Rowley MA, Thornton EA (1996) J Eng Mater Technol Trans ASME 118:19
10. Shi S, Jordan EH, Walker KP (1992) Int J Soli Struc 29:2663
11. Miner RV, Castelli MG (1992) Metall Trans A 23:551. doi:10.1007/BF02801173
12. Wanjaraa P, Jahazia M, Monajatib H, Yueb S, Immarigeona JP (2005) Mater Sci Eng A 396:50. doi:10.1016/j.msea.2004.12.005
13. Seshacharyulu T, Medeiros SC, Frazier WG, Parasad YVRK (2000) Mater Sci Eng A 284:184. doi:10.1016/S0921-5093(00)00741-3
14. Dieter GE (1984) Workability testing techniques. American Society for Metals, Ohio, p 58
15. Mataya MC, Sackschewsky VE (1994) Metall Trans A 25:2737. doi:10.1007/BF02649226
16. Park NK, Kim IS, Na YS, Yeom JT (2001) J Mater Proc Tec 111:98. doi:10.1016/S0924-0136(01)00489-7
17. Moneteillet F, Jonas JJ (1996) Metall Mater Trans 27A:3346
18. Semiatin SL, Weaver DS, Fagin PN, Glavicic MG, Gotez JR, Frey ND, Kramb PC, Antony MM (2004) Metall Mater Trans 35A:679
19. Henderson DW (1979) J Non-Cryst Sol 53:301. doi:10.1016/0022-3093(79)90169-8
20. Ruitenberg G, Woldt E, Petford-Long AK (2001) Thermochimica Acta 371:97. doi:10.1016/S0040-6031(01)00584-6
21. Christian JW (1975) The theory of transformations in metals and alloys part I. Pergamon Press, Oxford
22. Sharma RC (2002) Phase transformations in materials. CBS publishers, New Delhi
23. Medeiros SC, Prasad YVRK, Frazier WG, Srinivasan R (2000) Scri Mater 42:17. doi:10.1016/S1359-6462(99)00316-4
24. Sims CT, Stoloff NS, Hagel WC (1987) Superalloys II. John Wiley & Sons, Inc., New York, NY